ORIGINAL ARTICLE

Analysis of landslide susceptibility and potential impacts on infrastructures and settlement areas (a case from the southeastern region of Türkiye)

Candan Gokceoglu[1] · Gizem Karakas[2] · Nazlı Tunar Özcan[1] · Aziz Elibuyuk[3] · Sultan Kocaman[2]

Abstract

Landslides have harmful effects not only on buildings but also on infrastructure and the natural environment. While they are typically triggered by natural events, such as heavy rainfalls and earthquakes, landslides can also be induced by anthropogenic activities, such as excavation and blasting. In certain regions, gigantic paleo-landslides exist, but triggering them is extremely difficult. However, triggering secondary landslides in gigantic paleo-landslides is relatively easy compared to the main corpus. The main purpose of this study was to produce a susceptibility map in a region in southeastern Türkiye and to discuss the impact of petroleum seismological investigation concerning the trigger of the landslides. For this purpose, a landslide inventory was compiled using geospatial data sets and field observations and used for landslide susceptibility mapping with the Random Forest algorithm. The accelerations sourced from blasting were also measured and the run-out distances were determined. A run-out distance map was produced using inverse distance weights. The study presents comprehensive insights by integrating a landslide susceptibility map and run-out distance map. It evaluates the impact of blasting on landslides through in-situ measurements and slope stability analyses. Findings indicate that no triggering effect on landslides was observed if the dynamite quantity remains below 4 kg and the blasting distance exceeds 10 m from the landslide.

Keywords Landslide · Blasting · Run-out · Siirt (Türkiye) · Susceptibility

✉ Sultan Kocaman
sultankocaman@hacettepe.edu.tr

Candan Gokceoglu
cgokce@hacettepe.edu.tr

Gizem Karakas
gizem.karakas@hacettepe.edu.tr

Nazlı Tunar Özcan
ntunar@hacettepe.edu.tr

Aziz Elibuyuk
aziz.elibuyuk@calikpetrol.com

[1] Department of Geological Engineering, Hacettepe University, Beytepe, 06800 Ankara, Türkiye

[2] Department of Geomatics Engineering, Hacettepe University, Beytepe, 06800 Ankara, Türkiye

[3] Çalık Petrol, Ak Plaza, Söğütözü, Ankara, Türkiye

Introduction

Petroleum seismology as a specialized branch of seismology was developed in parallel with the growing demand for hydrocarbons, particularly oil and gas (Ikelle and Amundsen 2005). Thanks to the advancements in petroleum seismology, the exploration and identification of hydrocarbon reserves, evaluation of their properties, and monitoring of hydrocarbon production from reservoirs have become much easier. The use of seismic waves has enabled geologists and engineers to draw detailed images of the subsurface. These images provide critical information about the location, size, and characteristics of hydrocarbon deposits, such as trap geometry, degree of maturation, holding capacity, etc. (Liner and McGilvery 2019). During these studies, a systematic blasting process uses explosives such as dynamite to create the seismic waves required to interpret the subsurface. The seismic effects of blasting can resemble the shocks of a small earthquake (Dvorak 1978), thus making blasts triggering factors in materials susceptible to mass movements.

In the literature, several examples of instabilities caused by blasting and damage to infrastructures can be found.

Cui et al. (2022) reported a catastrophic landslide in a karstic area in Nayong (Guizhou, China) that resulted in the death of 35 people. The main triggering factor for this landslide was the blasting in a coal mine operated by an underground mining system near the area of mass movement (Xiong et al. 2022). The seismic waves produced by blasting activities caused the karstic discontinuities to enlarge and extend. Consequently, the bedrock on the slope was deformed, making the mass movement inevitable (Cui et al. 2022). During the construction of the subway line in Nanning, Guangxi, a blast occurred, resulting in the rupture of the main water supply pipeline. This caused nearby residential areas and streets to be submerged (Jiang et al. 2021). It is known that the landslides in Kattmarka (Norway, 2009), La Romaine (France, 2009), and Hawkesbury (Canada, 1955) were triggered by explosives used during excavation of highway slopes (Bouchard et al. 2016). Another striking example of landslides triggered by explosions occurred as a result of the operation carried out to distribute stacked logs in the Toulnustouc River, which yielded the loss of nine lives. Although the literature often discusses slope instabilities triggered by activities, such as mining and tunneling, as well as explosions in highway slopes, no studies have been found regarding instabilities resulting from explosions during seismic surveys conducted for oil exploration purposes.

The literature contains a large number of articles on the assessment and mapping of landslide susceptibility. Gokceoglu and Sezer (2009) predicted a rising trend in regional landslide susceptibility and hazard assessments. In line with this, numerous studies have been published reflecting the development of the methodologies used for producing landslide susceptibility maps. In the early stages of landslide susceptibility studies, simple map overlay approaches and statistical methods were commonly used (e.g., Gupta and Joshi 1990; Mehrotra et al. 1991; Pachauri and Pant 1992; Guillande et al. 1993; Gokceoglu and Aksoy 1996; Baeza and Corominas, 2011; Lee and Min 2001; Donati and Turini 2002). After this period, more advanced algorithms and methodologies such as logistic regression (i.eGorum et al. 2008; Lombardo and Mai 2018; Li et al. 2019; Xing et al. 2021; Das and Lepcha 2019), artificial neural networks (i.e. Choi et al. 2010; Poudyal et al. 2010; Nefeslioglu et al. 2012; Tsangaratos and Benardos 2014; Chen and Song 2023a, b), fuzzy and neuro-fuzzy algorithms (Ercanoglu and Gokceoglu 2002; Pradhan et al. 2010; Akgun et al. 2012; Pourghasemi et al. 2012; Ozer et al. 2020) and the other machine learning algorithms (i.e. Hong et al. 2019; Shirvani 2020; Dang et al. 2020; Can et al. 2021; Zhao et al. 2021; Karakas et al. 2022; Chen et al. 2023; Kaya Topacli et al. 2024; Karakas et al. 2024) have been utilized. Consequently, this brief literature survey revealed that the regional landslide susceptibility assessment studies represent an essential and ongoing research area.

In recent years, rapid exploration of new resource areas has continued to meet the growing energy demand. Petroleum reserves have been discovered in the coastal areas of synclines in the sedimentary basins located in the Southeastern Anatolia Region of Turkiye (Alparslan and Koca 2012). At the time of this writing, there are active oil wells in Batman, Diyarbakır, and Siirt provinces located in the Southeastern Anatolia Region, and these wells are operated by Turkish Petroleum Corporation (TPAO) and private companies. In addition, various licensed areas are actively conducting seismic surveys to continue the exploration of oil reserves. Çalık Petrol Corporation plans to start oil exploration in one of these licensed areas, Tillo, Siirt, where seismic studies are scheduled to take place. In addition to a number of small settlements, the area also contains important engineering structures, such as the Alkumru Dam and the Kirazlık Regulator. The dam and the regulator produce electricity. However, there are extra-large extending paleo-landslides around these engineering structures. In these huge paleo-landslides, some small- or moderate-sized actual landslides have developed.

The main objectives of this study were to prepare a landslide susceptibility map indicating the areas prone to landslides, to identify the seismic triggering thresholds, and to determine the run-out distances in the event of landslides in the region. To achieve these goals, a landslide inventory of the study area was compiled using aerial photographs, satellite images, and field observations. The statistical parameters related to landslides (slope, altitude, aspect, lithology, etc.) were derived and a landslide susceptibility map was produced using the random forest (RF) method. In addition, in-situ measurements were conducted to determine the accelerations and particle velocities that may occur during the blasting. Consequently, this study has the potential to provide new insights into the regional assessment of the extremely complex natural hazard, such as landslides.

In the following, the regional characteristics were presented followed by the seismic investigations and in-situ measurements. The landslide susceptibility mapping and the run-out distance computation and mapping approaches were discussed in Sects. "Landslide Susceptibility Mapping" and "Discussion". The final section highlights the main findings and conclusions of the study.

General characteristics of the study area

The study area is located in the southeastern part of Türkiye near the city of Siirt (Fig. 1). Botan River, tributary of the Dicle River flows through the study area and involves the Alkumru Dam and Kirazlık Regulator. The Alkumru Dam
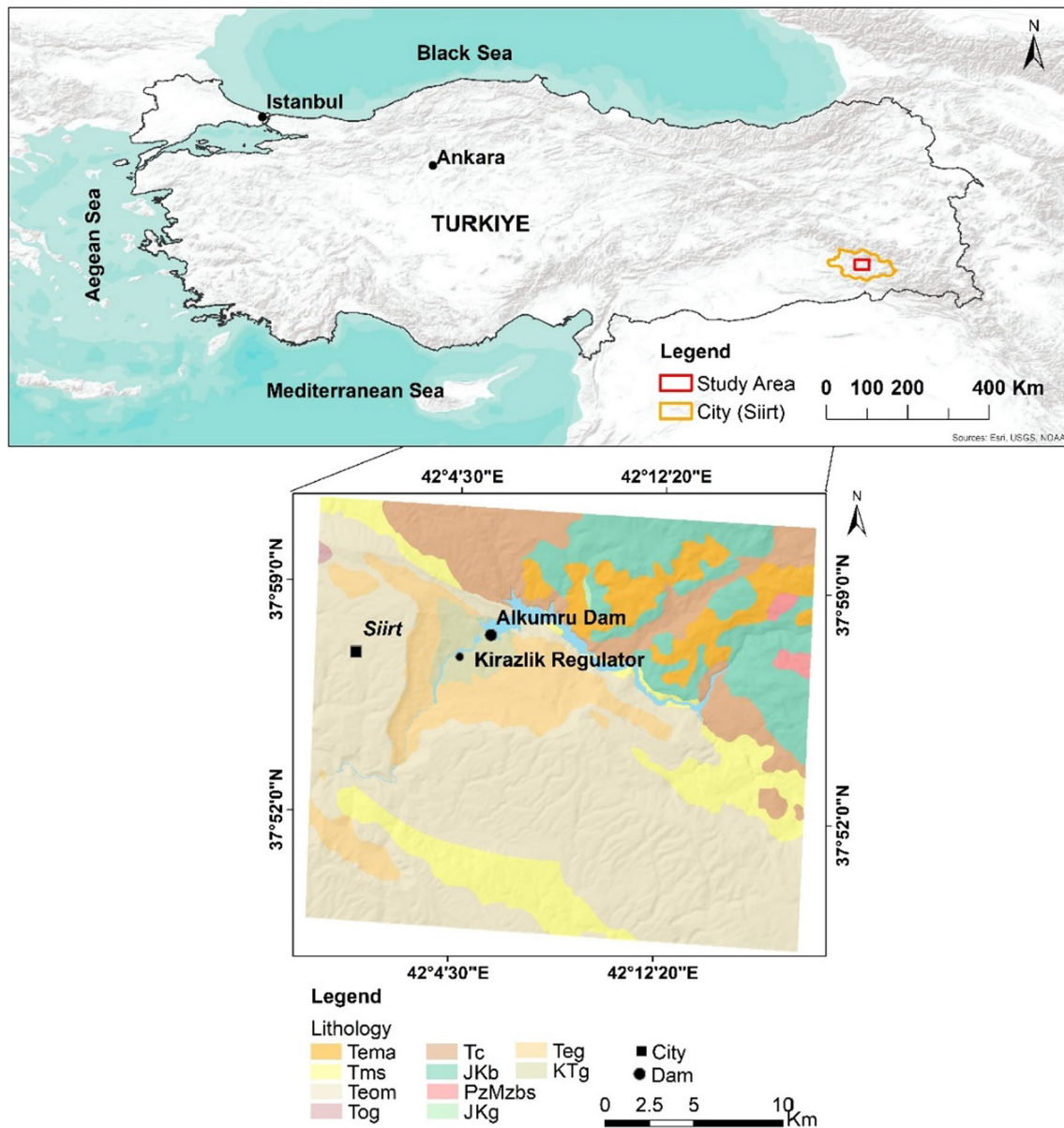
Fig. 1 Location and geological map of the study area (Modified from Şenel 2007)

has a crest elevation of 542 m and a height of 110 m. The Alkumru hydroelectric power plant, which has a total capacity of 280 MW, has an annual average generation capacity of 1 billion kWh. In 2017, the plant generated 720 million kWh (Limak Energy, 2022). The Kirazlık Regulator, a small-scale regulating dam, is located 8 km from the Alkumru Dam (Fig. 1).

The study area is located on the Pütürge–Bitlis–Zagros suture zone, which is one of the main tectonic structures of Türkiye. While the Pütürge–Bitlis–Zagros Suture Zone extends to the north of this belt, there is a metamorphic-based Arabian platform to the south (Fig. 2). Depending on the interplate compression regime, the metamorphic basement subducted under the Anatolian plate, while the Tertiary–Quaternary sedimentary units above it hit the suture zone and turned backward (south) and formed folds (Özgen et al. 2005). According to the geological map of Türkiye, Paleozoic, Mesozoic and Cenozoic aged sedimentary, metamorphic and magmatic rocks crop out in the Alkumru dam and its immediate vicinity (Fig. 2). There are nine different geological units in the region: Paleozoic and Jurassic marbles, Upper Cretaceous–Paleocene aged clastic and carbonate rocks, Triassic schists, calcschists, Eocene aged neritic rocks, continental clastics and volcanics (Fig. 1). The oldest geological unit in the vicinity of the study area is the Germav Formation (Maxon 1936), which is of the
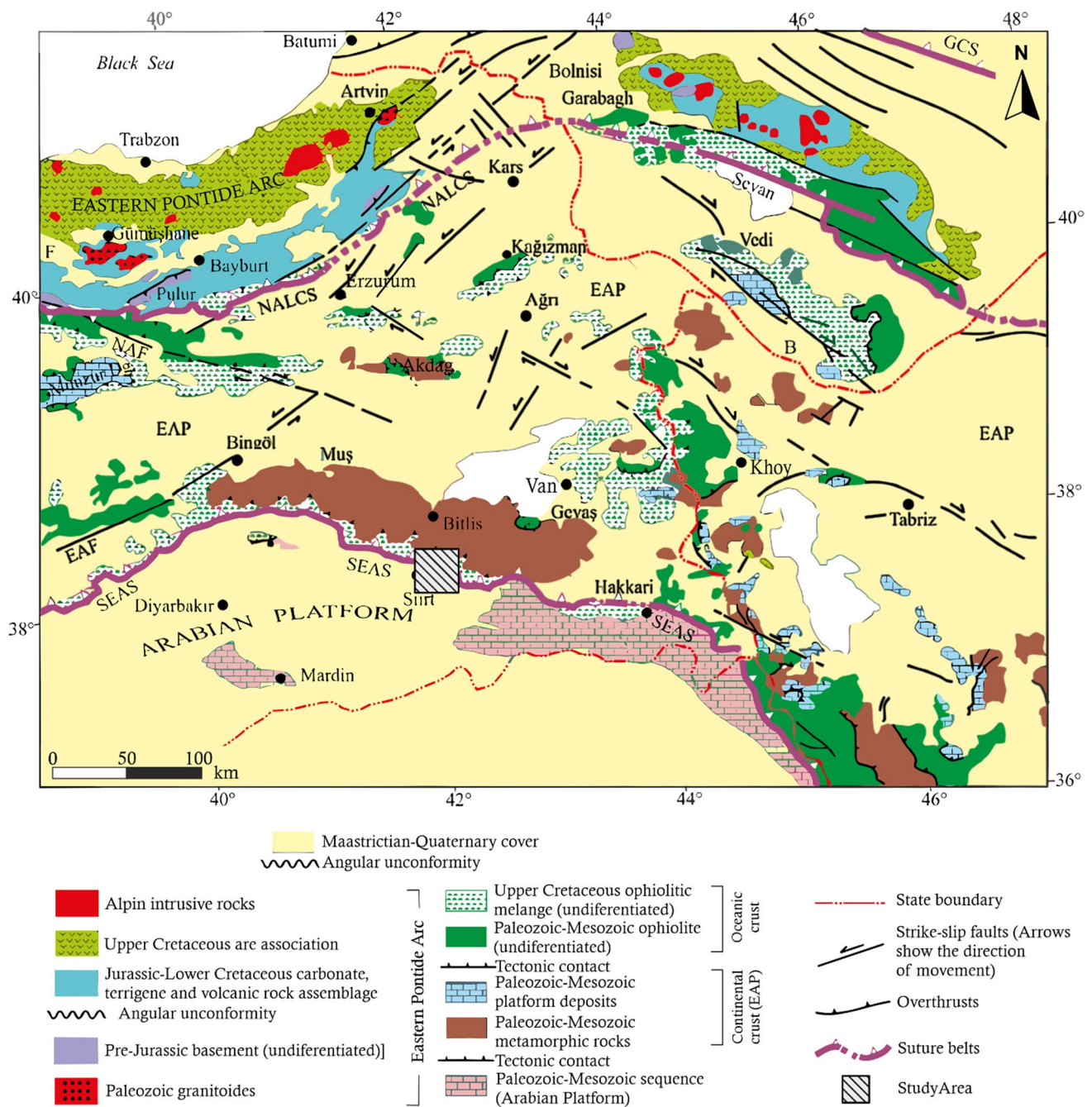
Fig. 2 General tectonic map of the East Anatolian Plateau (modified after Yilmaz et al. 2014)

Upper Cretaceous–Paleocene age. The Germav Formation, representing a deep sea slope environment, typically includes units composed of an alternation of grey-colored sandstone, marl, and shale, with intercalations of limestone (Güven et al. 1991). The Gercüş Formation, which is of the Paleocene–Early Eocene age and consists of a sequence of reddish mudstone, sandstone, and claystone, conformably overlies the Germav Formation. Gercüş Formation consists of reddish marl, sandstone, and conglomerate sequences,

followed by reddish, occasionally greenish-gray, sandy, and clayey units (Duran et al. 1988). The Hoya Formation, which consists of deep-sea limestones of the Middle–Late Eocene age, overlies the Gercüş Formation. This geologic unit was deposited in a shallow sea, shelf edge, and/or fore-shelf environment (Duran et al. 1988). The Germik Formation, which is Oligocene-aged, is located on top of the Hoya Formation and consists of shallow marine deposits that transition both vertically and laterally with this formation. The Germik

Formation exhibits a depositional sequence that starts with a conglomerate in gentle slope areas, followed by fine- and coarse-grained detrital rocks, and occasionally ends with a top conglomerate (Özgen and Karadoğan 2013). Upper Miocene–Lower Pliocene aged Şelmo Formation unconformably overlies the Germik Formation and consists of a conglomerate, sandstone, and siltstone sequence (Dinç and Keskin 2017). The depositional environment of the Şelmo Formation has been determined as beach sands, transitional tidal flats, playa, and terrestrial (fluvial) (Duran et al. 1989).

The study area covers an area of approximately 662 km^2 and includes seven land use land cover (LULC) types. According to the WorldCover v2 product (ESA-WorldCover 2021) of European Space Agency (ESA), the areal percentages of these classes are as follows: tree cover (6.08%), shrubland (0.07%), grassland (79.65%), cropland (5.40%), built-up area (0.44%), bare/sparse vegetation (6.51%), and permanent water bodies (1.83%).

The geomorphology of the study area is affected by landslides and a typical hummocky topography is dominant (Fig. 3). After the initial great slope failures, the gigantic landslides stabilized. However, the actual landslides developed in the displaced and disturbed slope material due to large landslides and they are active (Fig. 4). The actual landslides are typical circular failures and depths of the failure surfaces are between 1 and 10 m.

The landslide inventory used here was also compiled in this study through visual interpretation of digital elevation model (DEM), aerial orthophotos, and satellite images freely provided on the Google Earth platform. In addition, in-situ assessments were carried out. The DEM was obtained from the EU-DEM v1.1 (CLSM 2023), which was freely available, and has 25 m spatial resolution and approximately 7 m vertical accuracy. A total of 364 landslides were inventoried in the study area. The surface areas of the largest and smallest landslide were 3.05 km^2 and

Fig. 4 View from a landslide observed in the study area

0.00064 km^2, respectively. The distribution of the landslides in the study area is shown in Fig. 5.

The size distribution of landslides is important when quantifying their occurrence and magnitude (Guzzetti et al. 2002; Malamud et al. 2004; Qiu et al. 2021). For this reason, several researchers, such as Tanyas et al. (2018), Fan et al. (2019), Huang and Yao (2021), Karakas et al. (2021), Ju et al. (2023) assessed the landslide frequency–area distributions for different regions. In this study, the power-law relationship for the identified landslides was derived, as shown in Fig. 6. The rollover effect and fractal dimension were determined as 0.0004 km^2 and – 1.416, respectively.

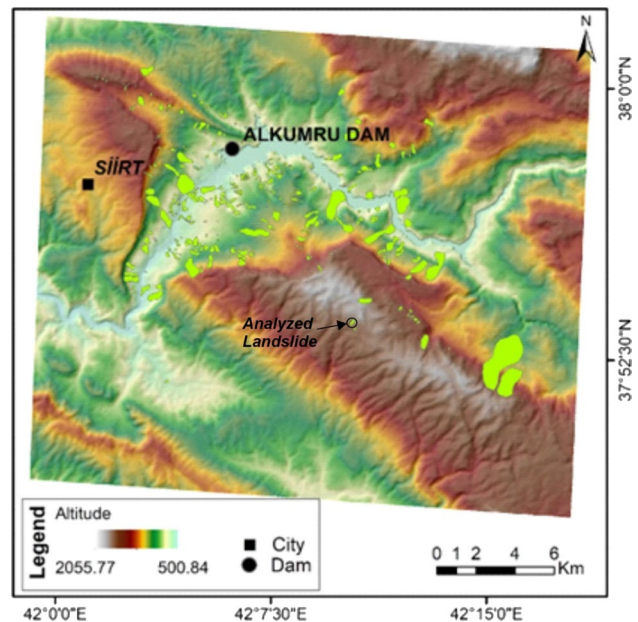**Fig. 3** Overview photo of a part of the study area

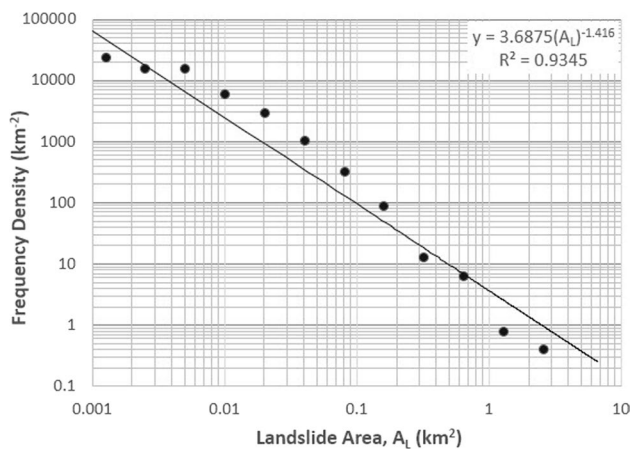**Fig. 5** Distribution of the landslides in the study area

Fig. 6 Relationship between area (size) and frequency values of landslides in the study area

Seismic investigations and in-situ measurements

For the oil investigation, seismic measurements along 200 km lines (Fig. 7) were planned in the study area. During the seismic measurements, blasting was utilized with very low amounts of dynamite (1–4 kg) placed in plastic casings of 30–40 cm in length and 3–5 cm in diameter, inserted into wells approximately 11 cm in diameter and up to 20 m in length. A high particle speed was achieved (5800–6300 m/s) with the study aimed at creating minimum phase seismic signals. The Vibro, which is used as a vibrating seismic source, gen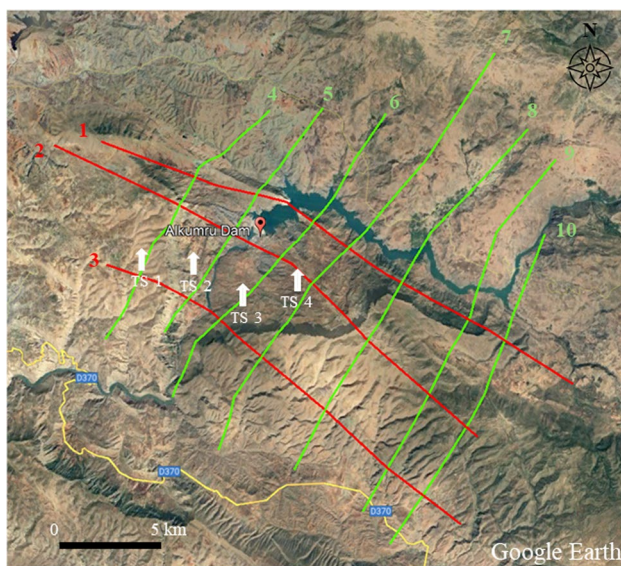erates a zero-phase seismic signal with controllable frequency content and provides a controlled energy source (Calik Energy 2020). To determine the horizontal acceleration and its attenuation, in-situ trial blastings and seismic measurements were performed by experts. Four locations were selected for trial blasting. The plan involved placing seismic measurement devices at intervals of 10 m, 50 m, and 100 m along two perpendicular lines, adhering to this rule as much as possible within the constraints of field conditions.

Landslides are frequently triggered by rainfall and seismic activity. Hence, we focused on investigating the acceleration, velocity, and their variations with distance during the planned blasting within the scope of seismic studies. Considering the size of the area and the large number of landslides (364), conducting detailed stability analyses for each landslide individually was not feasible due to time and financial constraints. Therefore, relevant seismic parameters were obtained to perform a general assessment. Accordingly, the data obtained from the measurements were evaluated. The maximum particle velocity–distance graph obtained from trial blastings is given in Fig. 8, illustrating all the data. As can be seen in Fig. 8, there is an exponential attenuation relationship between maximum particle velocity and distance. When 5 kg of dynamite was used, a velocity of 202.6 mm/s was measured within the first 10 m, while 201.4 mm/s was measured at the same distance as 6 kg of dynamite. On the other hand, the maximum amount of dynamite to be used in seismic studies is 4 kg, and the highest velocity measured for this amount is 182.1 mm/s. However, as can be seen in Fig. 8, these amounts rapidly drop below 25 mm/s in the first 15 m distance. According to the classification given by Oriard and Emmert (1980), 25 mm/s is the upper limit of discomfort. Therefore, no damage is expected at speeds lower than 25 mm/s. In addition, maximum horizontal acceleration, which is an important parameter for the stability of slopes during blasting, was also measured. The highest acceleration during the trial blasts was obtained when 2 kg of dynamite was used at the Test 4 station. This
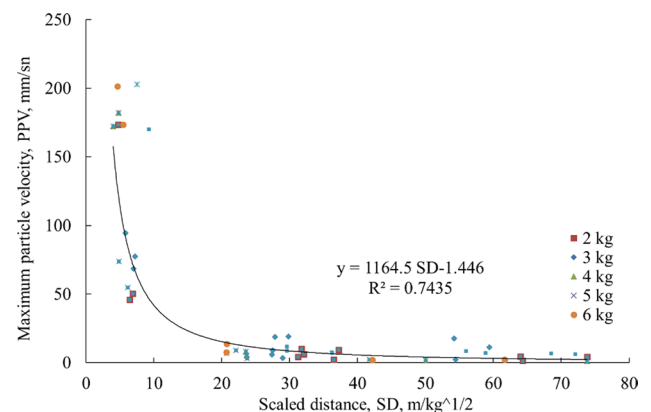

Fig. 7 Seismic investigation lines (planned)

Fig. 8 Relationship between maximum particle velocity and distance

value is 4.5 gal (0.0045 g) and was obtained at a point, where the ground was extremely loose. As can be seen from Fig. 9, the acceleration value drops to 0.002 g in the first 15 m and loses its effect in a short distance.

As stated previously, rotational types of landslides are typical in the study area. However, it is impossible to apply slope stability analysis on all landslides. Hence, an in-depth analysis of a chosen landslide (please see Fig. 5 for its location) was conducted to comprehend the impact of acceleration resulting from blasting. A slope resembling one of the landslides found in the field was utilized for this purpose. The unit weight, cohesion, internal friction angle, and pore water pressure (r_u) of the material forming the slope were taken as 18 kN/m^3, 25 kPa, 8 degrees, and 0.3, respectively. Under static conditions, the factor of safety was obtained as 1.125 (Fig. 10a). When the same slope was analyzed with 0.14 g, which is half of the highest ground acceleration for the field, 0.287 g, the factor of safety decreases to 0.761 and the slope loses its stability (Fig. 10b). When the same slope was reanalyzed using the highest horizontal ground acceleration measured during blasting in the field, the factor of safety drops to 1.109 (Fig. 10c). In other words, the decrease in the factor of safety is around 1.5% due to blasting.

Landslide susceptibility mapping

In this section, the conditioning factors and the methods used for the landslide susceptibility map (LSM) production were explained. The results were discussed accordingly.

Landslide conditioning parameters

In the present study, the predictors used for the production of LSMs for the landslides can be categorized as topographic (altitude, aspect, slope, plan and profile curvature, stream power index, topographic wetness index, drainage

Fig. 9 Relationship between horizontal acceleration and distance

density) and geological (lithology, see Fig. 1). The predictors and their base data sources used are given in Table 1. The predictors were chosen based on expert opinion, the regional characteristics of the study area, and an analysis of the literature. The topographic predictors were extracted using ArcGIS software from ESRI, Redlands, CA, USA, and open-source System for Automated Geoscientific Analyses (SAGA) tool (Conrad et al. 2015). The slope, aspect, plan, and profile curvatures, drainage density, topographic wetness index (TWI), and stream power index (SPI) from topographic predictors were computed from the 25 m resolution EU-DEM v1.1 (CLSM, 2023) (see Fig. 5). The lithology parameter, one of the most crucial factors in landslide formation, was obtained by digitizing the 1/100,000 scale geological maps published by Şenel (2007). After the digitization process, identifier (ID) numbers were assigned to the vector polygons defining the lithological units in preparation for the rasterization process. A rasterized lithology map was produced according to the ID values ranging between 1 and 10. The lithological units and their corresponding areas are provided in Table 2. The most frequently observed lithological unit in the study area is the Midyat group (undifferentiated), followed by Selmo formation, Cüngüs formation, Cergus formation and Maden formation.

Slope, as the first derivative of altitude, is an essential parameter in the LSM production, as landforms with higher slope angles are more susceptible to landslides. It is determined by the rates of change of the surface in both horizontal and vertical directions from the central cell. Aspect defines the direction of the downhill slope for each location. The aspect values represent the compass direction of the surface facing at that particular location, expressed in positive degrees between 0 and 360 measured clockwise from the north. Plan and profile curvatures as the second derivatives of altitude express the magnitude of the change in aspect and slope. The profile curvature parallel to the slope indicates the direction of the maximum slope, while the plan curvature is perpendicular to the direction of the maximum slope. The TWI is used to express the location and size of water-saturated areas. The formula proposed by Moore et al. (1991) (see Eq. 1) was used for calculating the TWI. The SPI (see Eq. 2) is a measure of the erosive power of flowing water. The places where the flow power index value is high indicate potential areas for high-velocity flows (Gokceoglu et al. 2005). The A_s and β values given in Eqs. 1 and 2 denote the basin area and slope, respectively. Drainage density, the ratio of the total length of rivers in the basin to the basin area, indicates the degree of surface flow, with higher drainage density suggesting greater surface flow (Nagarajan et al. 2000). Hydrology tool in ArcGIS software from ESRI, Redlands, CA, USA was used for producing the drainage density map from EUDEM v1.1 data:
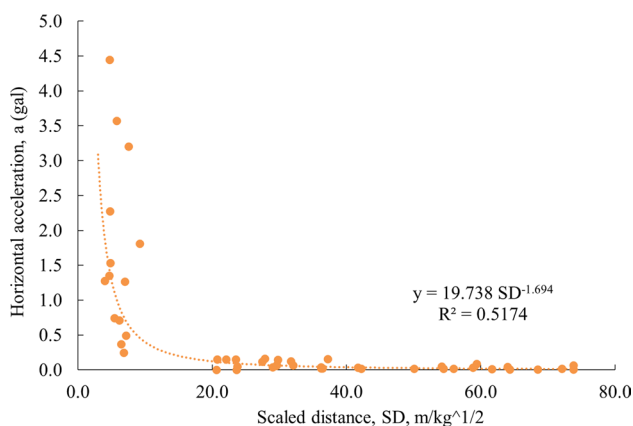
Fig. 10 Results of the slope stability analyses **a** under static conditions; **b** under dynamic conditions for expected earthquake; **c** under dynamic conditions for blasting
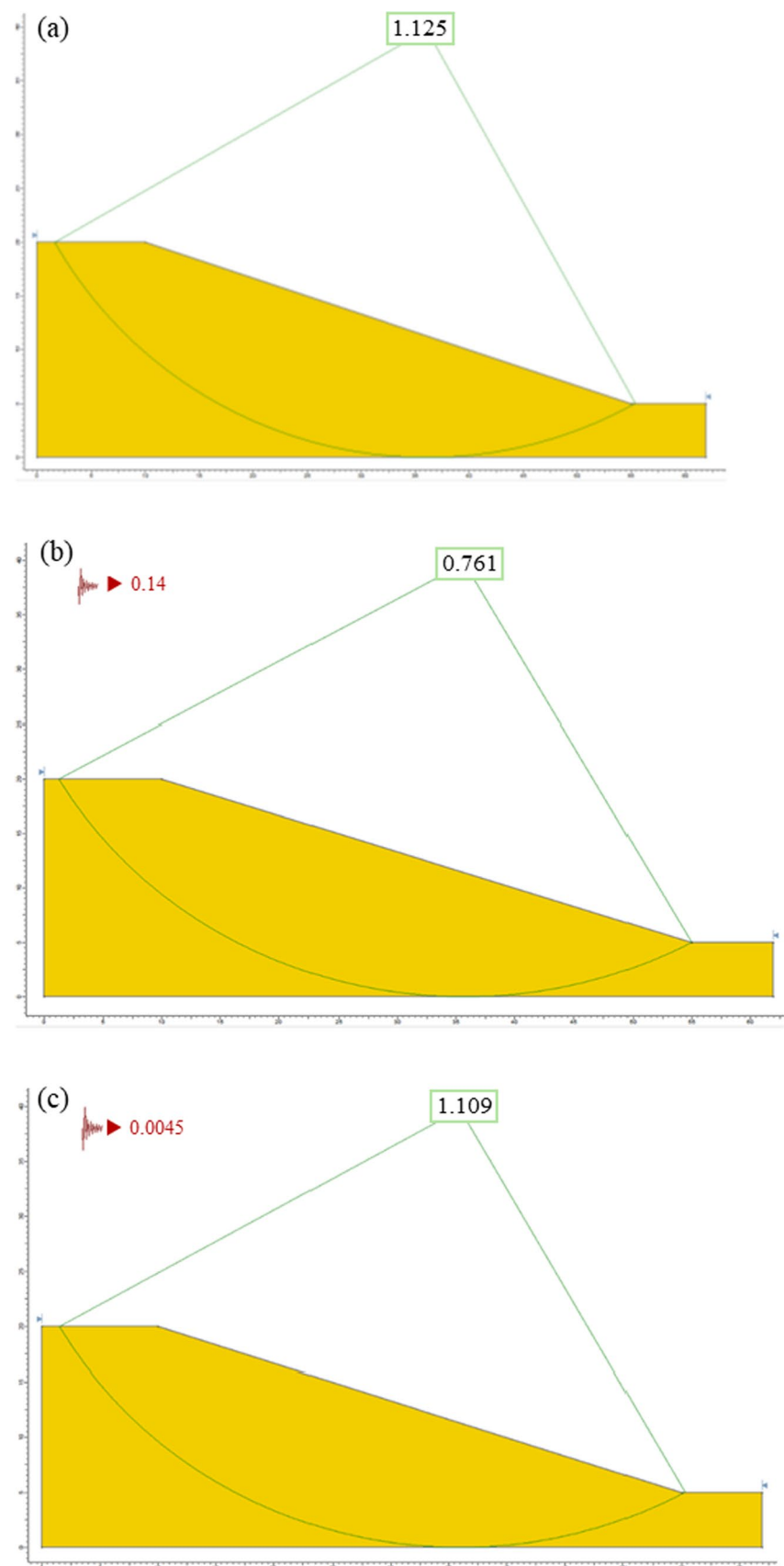
Table 1 Landslide predictors and their data sources used in the study

Category	Predictors	Sources	Resolution/Scale	Data type (Format)
Topographical Predictors	Altitude	EUDEM v1.1 by the Copernicus programme	25 m	Grid
	Slope	Derived from EUDEM v1.1	25 m	Grid
	Aspect			
	Plan and profile curvature			
	TWI			
	SPI			
	Drainage density			
Geological Predictor	Lithology	Geological maps published by Şenel (2007)	1/100,000	Polygon

Table 2 Lithological units and areas in the study area

ID	Symbol	Lithological unit	Area (km^2)
1	Tema	Maden formation:Conglomerate, sandstone, claystone, limestone, basalt, spillite	39.70
2	Tms	Selmo formation:conglomerate, sandstone, claystone (continental)	72.62
3	Teom	Midyat group (undifferentiated): Limestone, dolomite, clayey limestone, locally continental sandstone at the bottom	312.33
4	Tog	Germik Formation: Gypsum, shale, marl, dolomite	0.71
5	Tc	Cüngüs Formation: Sandstone, claystone, siltstone	71.98
6	JKg	Guleman Ophiolite: Serpentinite, serpentinized harzburgite and dunite, gabbro	0.43
7	PzMzbs	Schist, phyllite, quartzite, quartz schist	3.83
8	JKg	Guleman Ophiolite: Serpentinite, serpentinized harzburgite and dunite, gabbro	0.43
9	Teg	Gercus Formation: Marl, sandstone, claystone, conglomerate	69.20
10	KTg	Germav Formation: Shale, marn, sandstone	15.60

$$\text{TWI} = \ln\left(\frac{A_s}{\tan}\right) \tag{1}$$

$$\text{SPI} = A_s x \tan\beta. \tag{2}$$

The maps of eight conditioning factors are given in Fig. 11 (the lithology map was given in Fig. 1). When the LULC classes in the study area were analyzed, it was evident that the area primarily consists of the grassland class, constituting approximately 80% of the total area, as stated in Sect. "General Characteristics of the Study Area". In a study conducted by Karakas et al. (2022) in a neighboring site, it was found that the LULC feature did not significantly affect model accuracy. Since approximately 80% of the area consists of the grassland class and its impact on model accuracy was negligible, the LULC feature was not included in the model training for this study. Statistical parameters were derived for all predictors for the whole study area (Table 3) and for the landslide inventory polygons (Table 4) based on pixel values. While the study area has a mean altitude of 1120.3 m, the landslide regions have a mean altitude value of 925.3 m. The mean slope inside the landslides was 18.17° with a standard deviation (σ) of 8.97°. The mean

aspect (154°) and its σ (119°) indicate that the majority of landslides face east, south–east, south, and south–west directions. The statistical values can serve as additional measures for charactering landslides.

Landslide susceptibility mapping and performance assessment approach

The RF classifier (Breiman 2001) has been frequently employed for the LSM production due to its outstanding performance. It generates multiple decision trees during parameter training and selects the highest score among many independent trees. The most significant predictors were chosen from all trees for classification also by avoiding the correlation. Parameter optimization is crucial in the implementation so that the model can be trained as effectively as possible from the learning data set. Here, the RandomizedSearch technique was implemented for optimization (Randomized Search CV 2023). A number of RF parameters, such as n_estimators, max_depth, max_features, min_samples_split, min_samples_leaf, criterion and class_weight were tuned here using Python scikit-learn library (Scikit-learn 2023). The optimal values obtained from the RandomizedSearch are presented in Table 5.

The training and test data sets encompass all pixels inside the landslide polygons in the study area for landslide samples, while non-landslide samples were chosen at random locations outside of the inventory. A total of 721,872 pixels, comprising 32,083 landslide and 48,125 non-landslide pixels for each of the 9 predictors, were used in training. 80/20 ratio was utilized to split training and test samples. The performance of the RF classifier was then assessed using the test data set. The receiver operating characteristic curve (ROC), the area under ROC curve (AUC), and further statistical measures were computed

to evaluate the performance of the model. In addition, feature importance was assessed based on mean decrease in impurity (MDI) value obtained from the method. Finally, the landslide susceptibility values for the study area were computed from the trained RF model. A further data classification was performed using the natural breaks classification (Jenks) method (ArcGIS) to produce the LSM from the landslide susceptibility values. With this method, five susceptibility classes, such as very low, low, moderate, high, and very high, were formed based on the groups inherent in the data.
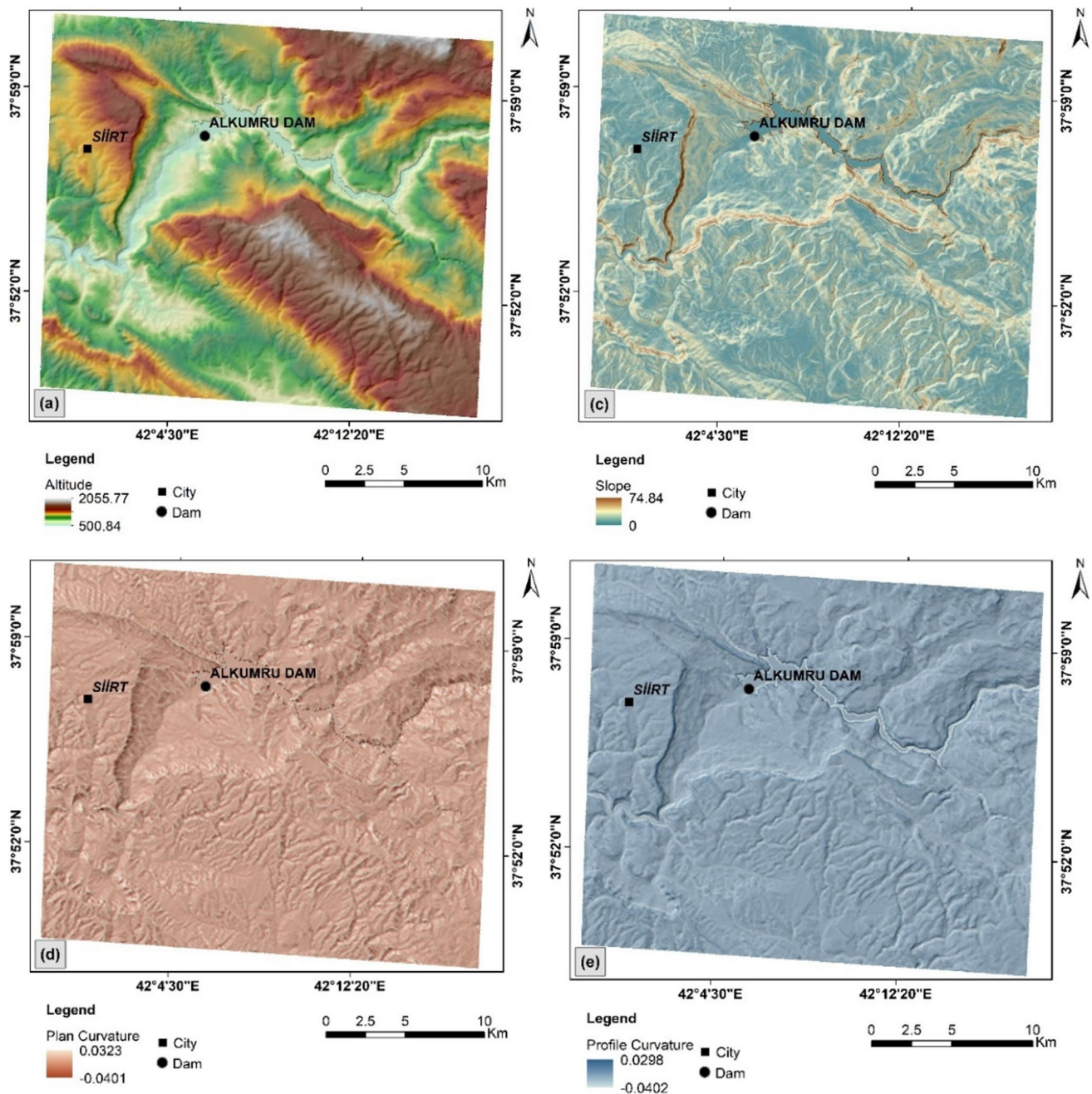

Fig. 11 Maps of predictors used for the LSM production: (**a**) altitude, (**b**) aspect, (**c**) slope, (**d**) plan curvature, (**e**) profile curvature, (**f**) drainage density, (**g**) SPI, (**h**) TWI
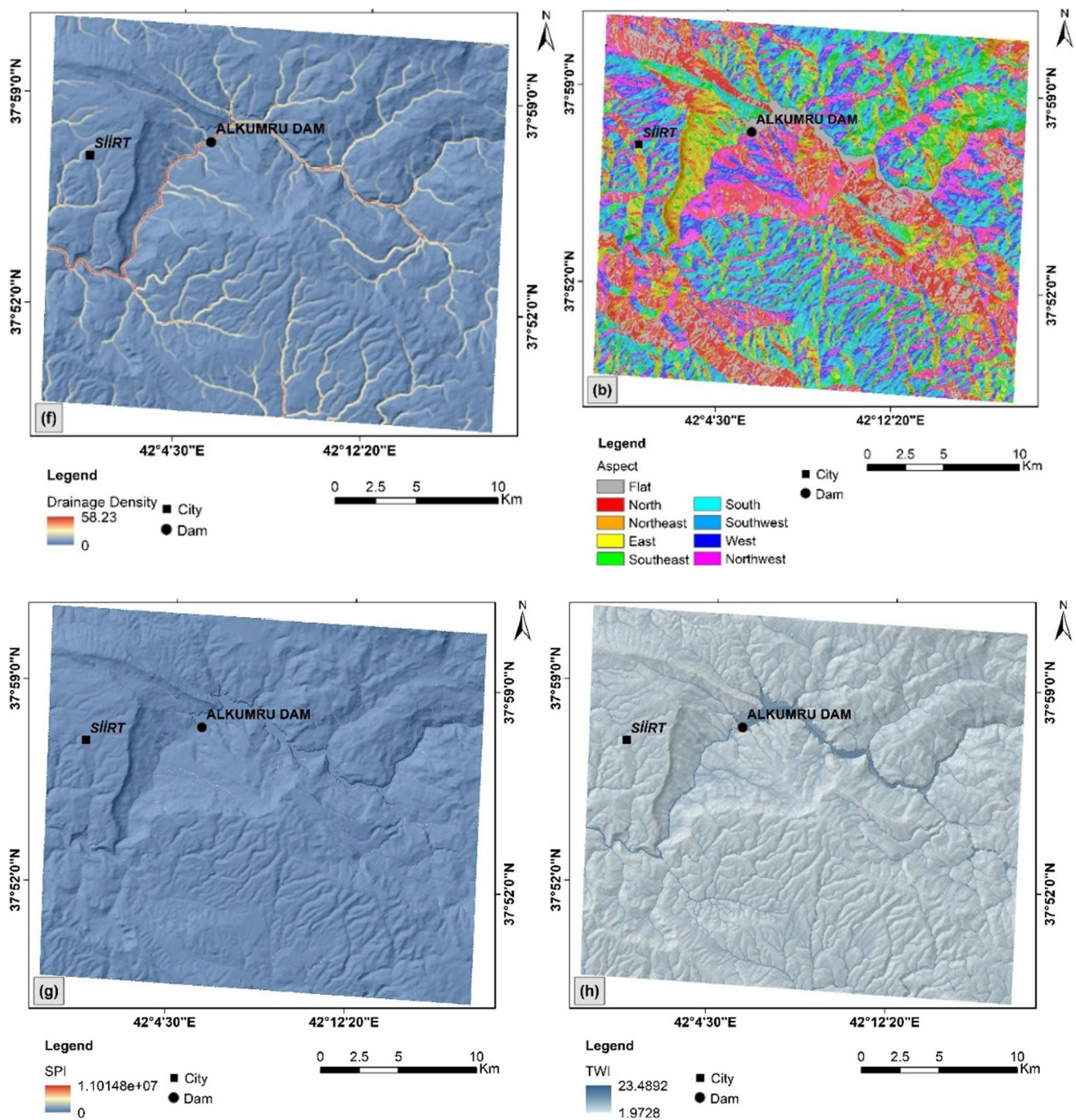
Fig. 11 (continued)

Landslide susceptibility map and the accuracy results

The predictive performance result of this study is illustrated in Fig. 12. The model accuracy was evaluated with the AUC values, visual interpretation of the ROC, and the widely used statistical measures (precision, $F1$ score, recall). The AUC and the overall accuracy (OA) values obtained from the

model were 0.95 and 0.89, respectively. Table 6 shows the accuracy measures of landslide and non-landslide classes separately. The results indicate higher accuracy of the non-landslide class, which can be expected due to their greater existence.

Figure 13 shows the LSM produced with the RF model. As can be seen in Fig. 13, the areas around the Alkumru Dam are highly susceptible to landslides. In addition, the

Table 3 Statistical summary of the predictors for the whole study area

Predictor	Min	Max	Mean	Std. Dev	Median
Altitude (m)	500.84	2055.77	1120.32	308.90	1082.25
Slope (°)	0	74.841	14.549	9.176	12.806
Aspect (°)	0	360	181.797	100.501	191.802
Plan curvature	− 0.040	0.032	5.29E–05	0.001	4.41E–05
Profile curvature	− 0.040	0.029	− 5.38E–05	0.001	− 2.10E–05
TWI	1.972	23.489	7.243	2.221	6.693
SPI	0	11,014,790	5,270.530	38,764.990	370.680
Drainage density	0	58.227	1.498	4.377	0

Table 4 Statistical summary of the predictors within the landslide inventory area
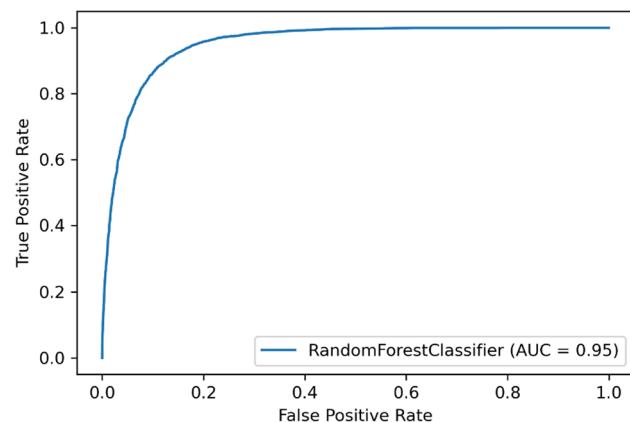
Predictor	Min	Max	Mean	Std. Dev	Median
Altitude (m)	513.33	1830.51	965.28	262.25	949.82
Slope (°)	0	69.437	18.168	8.972	16.879
Aspect (°)	0	360	154.042	119.012	119.510
Plan curvature	− 0.029	0.021	− 0.0001	0.001	− 0.0001
Profile curvature	− 0.028	0.021	− 0.0001	0.001	− 0.0001
TWI	2.543	23.209	7.445	1.745	7.177
SPI	0	11,014,790	11,419.964	90,635.702	556.258
Drainage density	0	42.513	1.367	3.922	0

Table 5 Optimized parameter values for the implemented RF algorithm

Algorithm	Parameters	Best value
Random forest	n_estimators	434
	max_depth	50
	max_features	'sqrt'
	min_samples_split	2
	min_samples_leaf	1
	criterion	'gini'
	class_weight	'balanced'

Table 6 Accuracy measures obtained from the RF classifier

Class	Precision	Recall	F1 Score
Non-landslide	0.92	0.89	0.90
Landslide	0.84	0.88	0.86

distribution and percentages of landslide probabilities for each class are given in Table 7. The area percentage of the landslide susceptibility classes of "very low", "low", "moderate", "high" and "very high" were 52.73%, 21.47%, 11.76%, 7.82%, and 6.22%, respectively. 25.8% of the study area was found prone to landslides at moderate to very-high levels.

The bar plot in Fig. 14 depicts the relationships between the model prediction and the predictors. The horizontal axis denotes the mean impurity value decrease for each predictor feature that is listed on the vertical axis. The predictors were ordered according to their importance values obtain from the MDI. In model prediction, the predictor with the greater percentage value is more significant. Thus, altitude (23%), lithology (14%), slope (13%), aspect (11%) and TWI (9%) were found to be more important than the other predictors.
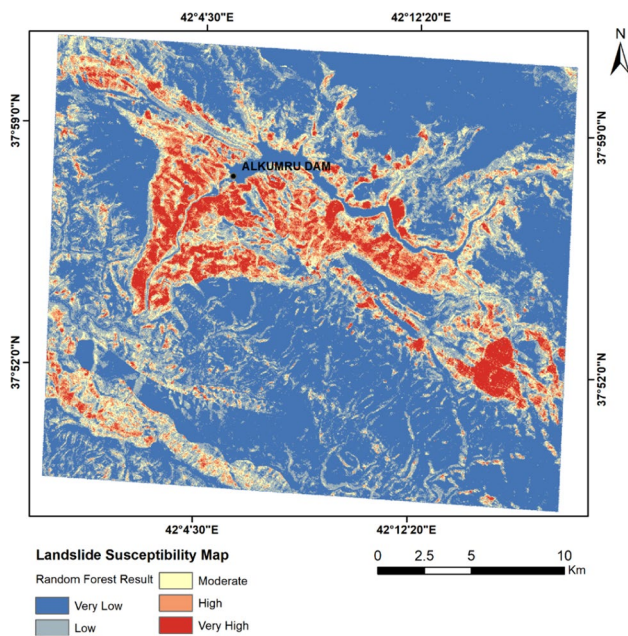

Fig. 12 RF model prediction performance illustrated as a ROC curve

Fig. 13 LSM produced with the RF model

Table 7 Ranges (class break values) of the landslide occurrence probabilities

Classes	Probability range (%)	Area (km^2)	Percentage (%)
Very high	71–100	41.17	6.22
High	47–71	51.75	7.82
Moderate	26–47	77.76	11.76
Low	9–26	142.00	21.47
Very low	0–9	348.77	52.73
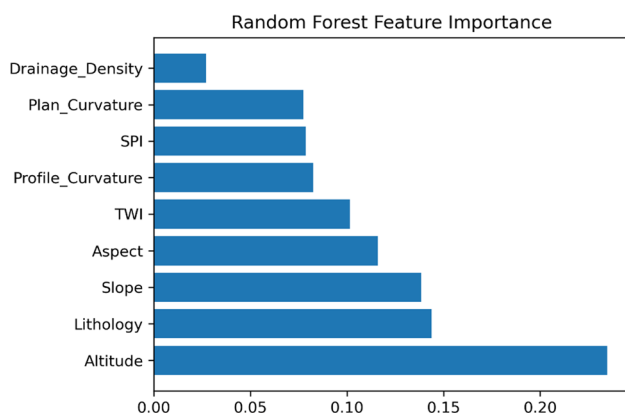
Fig. 14 Predictor importance obtained from the RF model
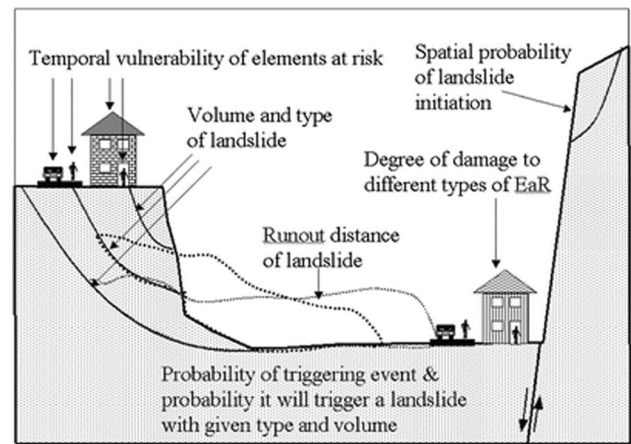
Fig. 15 Importance of run-out determination when assessing landslide risk (van Westen et al. 2005):

Run-out distances of landslides

Assessing landslide risk remains a challenging task, requiring evaluations of both susceptibility and hazard. While landslide susceptibility assessment has been conducted in this study, hazard assessment requires determining triggering mechanisms and thresholds. In this study, blasting-induced acceleration during seismic investigations was considered a possible trigger. However, the seismic acceleration values observed in the study area are insufficient to trigger a landslide.

Another crucial aspect of landslides is estimating run-out distances, as illustrated in a general sketch (Fig. 15) published by van Westen et al. (2005). The significance of run-out becomes apparent when considering the potential impact of landslides. One of the primary factors influencing landslide run-out is volume. Therefore, the volume of landslides was determined using the empirical formula (Eq. 3) proposed by Guzzetti et al. (2009), which is based on landslide area. In the initial stage, the areas of 364 landslides in the study area inventory were calculated. The histogram depicting landslide areas is presented in Fig. 16. The surface areas of the landslides in the study area range from 0.09 to 0.03 km^2. The volume of the smallest landslide was calculated to be 873 m^3, while the volume for the largest landslide was approximately 187 million m^3.

$$V_{\mathrm{L}} = 0.074 A_{\mathrm{L}}^{1.450}, \tag{3}$$

where V_{L} is the volume of landslide (m^3), and A_{L} is the area of landslide (m^2).

For the determination of the maximum landslide run-out distances, the empirical formula proposed by Legros (2002) was employed (Eq. 4). The maximum run-out distance was 935.5 m while the minimum run-out distance was calculated as

Fig. 16 Surface area distribution of landslides in the study area

Fig. 17 Run-out distance map of the study area
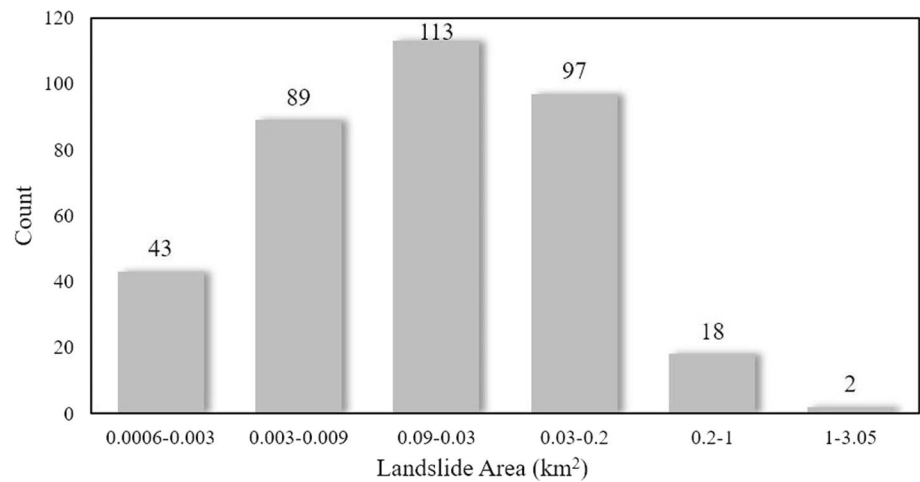
Discussion

In the present study, a comprehensive case study on landslides and their potential harmful effects is presented. An important aspect of the geomorphology in the study area is controlled by huge paleo-landslides. While these paleo-landslides have stabilized, some of the displaced material due to displacement was transported by the Botan River. However, numerous secondary landslides have developed in the displaced material along the slopes of the Botan River. The area was also subject to a petroleum seismic investigation, which involved the use of explosives, such as dynamite. In the initial phase of this study, the potential triggering effect of the explosions was analyzed. Subsequently, the effects of landslides if triggered were explored through susceptibility and run-out assessments. As can be seen from Fig. 17, the Alkumru Dam Body remains unaffected by the landslides. However, if triggered, the landslides have the potential to adversely affect the eastern parts of the dam reservoir. In addition, the Tosuntarla, Medreseköy, and Akmeşe villages in the southeastern part of the study area are under the landslide threat (Fig. 17). In the central part of the study area, the villages of Meydandere and Akyayla are also affected by the harmful effects of landslides. The roads connecting Koçlu and Meydandere, Alkumru dam–Meydandere, Tatlı–Pirinçli–Yaylacı–Tosuntarla–Medreseköy–Akmeşe are threatened by landslides (Fig. 17).
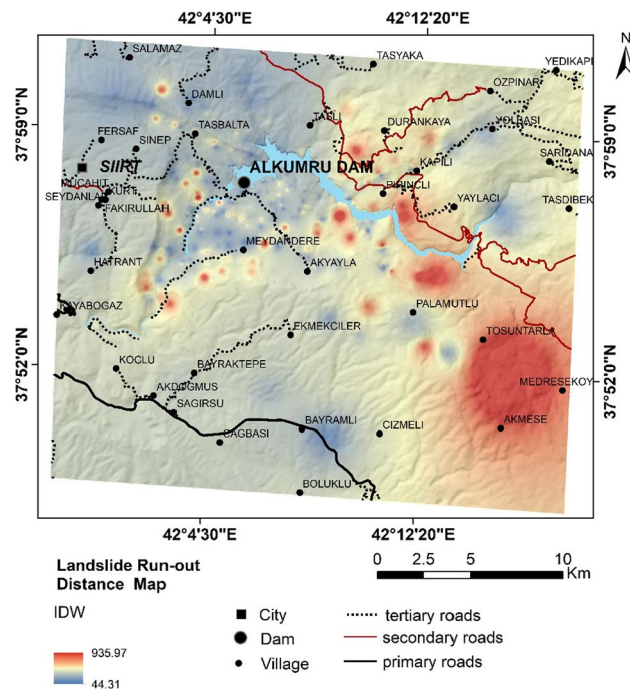
The presented study demonstrated the effective and safe petroleum seismic investigation in a landslide-prone area. Prior to the seismic investigation, an extensive landslide inventory study was performed, and in-situ geophysical measurements were taken to determine seismic parameters produced by the explosions. In addition, an LSM was produced, and the run-out distances of the landslides were determined and mapped. These maps and information were effectively utilized during the investigations, ensuring their safe completion. However, the study has limitations. The

43.5 m. The average value of the run-out distances computed from all landslides was 161.5 m. The run-out distance map for the study area was produced using the inverse distance weighting (IDW) method, and is shown in Fig. 17:

$$L_{max} = 8V_L^{0.25}, \tag{4}$$

where L_{max} is the maximum run-out distance (m), and V_L is the volume of the landslide (m^3).

main limitation is the determination of the threshold value of seismic acceleration for each landslide, which would require exhaustive geotechnical investigations and slope stability analyses for each landslide, making it infeasible given the number of landslides. Furthermore, the empirical determination of run-out distances for each landslide poses another limitation. Nevertheless, these limitations are acceptable as the study results were utilized during the investigation phase. Moreover, the results can be applied to select landslide-free areas for petroleum well locations. However, if a preferred location for a petroleum well is found to have landslides or is in a high landslide susceptibility class, additional geotechnical investigation and slope stability analyses are necessary.

Conclusions

This study presents an interesting case that investigates the possible harmful effects of seismic studies for oil exploration in an area with gigantic landslides. With numerous active landslides in the study area, the potential impacts on the natural environment, villages, agricultural areas, roads, and infrastructure such as dams and regulators are significant. The study aims to describe these potential harmful effects and propose necessary precautions. Based on the study outcomes, the following conclusions can be derived:

(a) An accurate landslide inventory was compiled through field investigations and by utilizing aerial and satellite images, and a DEM. A total of 364 landslides were inventoried with the largest and smallest areas of 3.05 km^2 and 0.00064 km^2.

(b) The inventory was employed for the landslide susceptibility map production with a widely used machine learning technique, the RF. An OA value of 89% was achieved from the test data set with an AUC value of 95%. These results indicate high quality of the LSM.

(c) The run-out distances of all landslides were computed with empirical methods and a run-out map for the study area was produced. Both maps may serve for site selection and taking the necessary precautions.

(d) An exponential attenuation relationship between maximum particle velocity and distance was observed. For instance, when 5 kg of dynamite was used, a velocity of 202.6 mm/s was measured within the first 10 m, while 201.4 mm/sec was measured at the same distance with 6 kg of dynamite. In addition, the highest acceleration during the trial blasts was recorded when 2 kg of dynamite was used at the Test 4 station. This value is 4.5 gal (0.0045 g) and was obtained at a point, where the ground was extremely loose. However, the acceleration value dropped to 0.002 g in the first 15 m and lost its effect in a short distance.

(e) A series of slope stability analyses were applied to understand the triggering effect of the measured accelerations on the landslides. Consequently, it was determined that if the amount of dynamite does not exceed 4 kg and the distance between the blasting point and landslide is at least 10 m, no triggering effect of blasting on the landslides occurs..

(f) This study provides a case discussing the effects of blasting on landslides. Blasting creates seismic acceleration, which can trigger landslides near the blasting point. Further research and additional data on this topic can enhance our understanding of the relation between blasting and landslides.

Declarations

References

Akgun A, Sezer EA, Nefeslioglu HA, Gokceoglu C, Pradhan B (2012) An easy-to-use MATLAB program (MamLand) for the assessment of landslide susceptibility using a Mamdani fuzzy algorithm. Comput Geosci 38(1):23–34. https://doi.org/10.1016/j.cageo.2011.04.012

Alparslan N, Koca D (2012) A general overview of geophysical methods used in petroleum exploration studies. Batman Univ J Life Sci 2:1

Baeza C, Corominas J (2011) Assessment of shallow landslide susceptibility by means of multivariate statistical techniques. Earth Surf Proc Land 26:1251–1263

Bouchard S, L'Heureux JS, Johansson J, Leroueil S, LeBoeuf D (2016) Blasting induced landslides in sensitive clays. Landslides and

Engineered Slopes, Experience, Theory and Practice – Aversa et al. (Eds), Associazione Geotecnica Italiana, Rome, Italy, ISBN 978-1-138-02988-0

Breiman L (2001) Random forests. Mach Learn 45:5–32

Calik Petrol Arama A.S. (2020) AR/ÇPA-HPE/M48-a1,a2,a3 Planned Steps to be Taken in and Around the Exploration License, Effects of 2D 2D Seismic Data Collection on Alkumru Dam and Kirazlı Regulator Located within the License Area. Internal Report, 15 (**in Turkish**)

Can R, Kocaman S, Gokceoglu C (2021) A comprehensive assessment of XGBoost algorithm for landslide susceptibility mapping in the Upper Basin of Ataturk Dam, Turkey. Appl Sci 11(11):4993. https://doi.org/10.3390/app11114993

Chen Z, Song D (2023) Modeling landslide susceptibility based on convolutional neural network coupling with metaheuristic optimization algorithms. Int J Digit Earth 16(1):3384–3416. https://doi.org/10.1080/17538947.2023.2249863

Chen Z, Song D, Dong L (2023) An innovative method for landslide susceptibility mapping supported by fractal theory, GeoDetector, and random forest: a case study in Sichuan Province, SW China. Nat Hazards 118:2543–2568. https://doi.org/10.1007/s11069-023-06104-9

Choi J, Oh HJ, Won JS, Lee S (2010) Validation of an artificial neural network model for landslide susceptibility mapping. Environ Earth Sci 60:473–483. https://doi.org/10.1007/s12665-009-0188-0

CLMS (Copernicus Land Monitoring Service) (2023) Website of CLMS. https://land.copernicus.eu. Accessed 3 Jan 2023

Conrad O, Bechtel B, Bock M, Dietrich H, Fischer E, Gerlitz L, Wehberg J, Wichmann V, Böhner J (2015) System for Automated Geoscientific Analyses (SAGA) v. 2.1.4. Geosci Model Dev 8(2):1991–2007

Cui FP, Li B, Xiong C, Yang Z, Penga J, Lia J, Lia H (2022) Dynamic triggering mechanism of the Pusa mining-induced landslide in Nayong County Guizhou Province, China. Geomatics Nat Hazards Risk 13(1):123–147

Dang VH, Hoang ND, Nguyen LMD, Bui DT, Samui P (2020) A novel GIS-based random forest machine algorithm for the spatial prediction of shallow landslide susceptibility. Forests 11(1):118. https://doi.org/10.3390/f11010118

Das G, Lepcha K (2019) Application of logistic regression (LR) and frequency ratio (FR) models for landslide susceptibility mapping in Relli Khola river basin of Darjeeling Himalaya, India. SN Appl Sci 1:1–22. https://doi.org/10.1007/s42452-019-1499-8

Dinç S, Keskin F (2017) Petrographic features of the units of hasankeyf and surrounding area (Batman). Batman Univ J Life Sci 7(2/2):23–35

Donati L, Turrini MC (2002) An objective method to rank the importance of the factors predisposing to landslides with the GIS methodology: application to an area of the Apennines disposing (Valnerina; Perugia, Italy). Eng Geol 63:277–289

Duran O, Şemşir D, Sezgin İ, Perinçek D (1988) Stratigraphy, sedimentology and petroleum potential of the Midyat and Silvan groups in the Southeastern Anatolia, Turkey. TPJD Bull 1(2):99–126

Duran O, Şemşir D, Sezgin L, Perinçek, D (1989) Stratigraphy, sedimentology and paleogeography of the Midyat Silvan Groups in the Southeastern Anatolia, Turkey: Paleontology, geological history, reservoir and diagenesis features and possible petroleum potential. TPAO Research Center, Report No. 2563.

Dvořák A (1977) Landslides caused by blasting. Bull Int Assoc Eng Geol 16:166–168. https://doi.org/10.1007/BF02591472

Ercanoglu M, Gokceoglu C (2002) Assessment of landslide susceptibility for a landslide-prone area (north of Yenice, NW Turkey) by fuzzy approach. Environ Geol 41:720–730. https://doi.org/10.1007/s00254-001-0454-2

Fan RL, Zhang LM, Shen P (2019) Evaluating volume of coseismic landslide clusters by flow direction-based partitioning. Eng Geol 260:105238. https://doi.org/10.1016/j.enggeo.2019.105238

Gokceoglu C, Aksoy H (1996) Landslide susceptibility mapping of the slopes in the residual soils of the Mengen region (Turkey) by deterministic stability analyses and image processing techniques. Eng Geol 44(1–4):147–161. https://doi.org/10.1016/S0013-7952(97)81260-4

Gokceoglu C, Sezer E (2009) A statistical assessment on international landslide literature (1945–2008). Landslides 6:345–351. https://doi.org/10.1007/s10346-009-0166-3

Gokceoglu C, Sonmez H, Nefeslioglu HA, Duman TY, Can T (2005) The 17 March 2005 Kuzulu landslide (Sivas, Turkey) and landslide-susceptibility map of its near vicinity. Eng Geol 81(1):65–83

Gorum T, Gonencgil B, Gokceoglu C, Nefeslioglu HA (2008) Implementation of reconstructed geomorphologic units in landslide susceptibility mapping: the Melen Gorge (NW Turkey). Nat Hazards 46(3):323–351

Guillande R, Gelugne P, Bardintzeff JM, Brousse R, Chorowicz J, Deffontaines B, Parrot JF (1993) Cartographie automatique de zones à aléas de mouvements de terrain sur ile de Tahiti à partir de données digitales. Bull Soc Géol Fr 4:577–583

Gupta RP, Joshi BC (1990) Landslide hazard zoning using the GIS approach—a case study from the Ramganga Catchment, Himalayas. Eng Geol 28:119–131

Güven A, Dinçer A, Tuna ME, Çoruh T (1991) Stratigraphy of the autochthonous Campanian-Paleocene succession in the Southeast Anatolia Region. TPAO Exploration Group, Report No. 2828.

Guzzetti F, Malamud BD, Turcotte DL, Reichenbach P (2002) Power-law correlations of landslide areas in central Italy. Earth Planet Sci Lett 195(3–4):169–183. https://doi.org/10.1016/S0012-821X(01)00589-1

Guzzetti F, Ardizzone F, Cardinali M, Rossi M, Valigi D (2009) Landslide volumes and landslide mobilization rates in Umbria, central Italy. Earth Planet Sci Lett 279(3–4):222–229

Hong H, Miao Y, Liu J, Zhu AX (2019) Exploring the effects of the design and quantity of absence data on the performance of random forest-based landslide susceptibility mapping. CATENA 176:45–64. https://doi.org/10.1016/j.catena.2018.12.035

Huang Y, Yao L (2021) Size distribution law of earthquake-triggered landslides in different seismic intensity zones. Nonlinear Processes Geophys 28:167–179. https://doi.org/10.5194/npg-28-167-2021

İkelle LT, Amundsen L (2005) Introduction to petroleum seismology. Investigations, Geophysics Series No. 12, Michael R. Cooper, series editor, Anthony F. Gangi, volume editör, Society of Exploration Geophysicists Tulsa, Oklahoma, USA

Jiang N, Zhu B, Zhou C, Li H, Wu B, Yao Y, Wu T (2021) Blasting vibration effect on the buried pipeline: a brief overview. Eng Fail Anal. https://doi.org/10.1016/j.engfailanal.2021.105709

Ju LY, Zhang LM, Xiao T (2023) Power laws for accurate determination of landslide volume based on high-resolution LiDAR data. Eng Geol 312:106935. https://doi.org/10.1016/j.enggeo.2022.106935

Karakas G, Nefeslioglu HA, Kocaman S, Buyukdemircioglu M, Yurur T, Gokceoglu C (2021) Derivation of earthquake-induced landslide distribution using aerial photogrammetry: the January 24, 2020, Elazig (Turkey) earthquake. Landslides 18:2193–2209. https://doi.org/10.1007/s10346-021-01660-2

Karakas G, Kocaman S, Gokceoglu C (2022) Comprehensive performance assessment of landslide susceptibility mapping with MLP and random forest: a case study after Elazig earthquake (24 Jan 2020, Mw 6.8), Turkey. Environ Earth Sci 81:144. https://doi.org/10.1007/s12665-022-10225-y

Karakas G, Unal EO, Cetinkaya S, Tunar Ozcan N, Karakas VE, Can R, Gokceoglu C, Kocaman S (2024) Analysis of landslide

susceptibility prediction accuracy with an event-based inventory: The 6 February 2023 Turkiye earthquakes. Soil Dyn Earthq Eng 178:108491. https://doi.org/10.1016/j.soildyn.2024.108491

Kaya Topacli Z, Ozcan AK, Gokceoglu C (2024) Performance comparison of landslide susceptibility maps derived from logistic regression and random forest models in the Bolaman Basin, Türkiye. Nat Hazard Rev 25(1):04023054. https://doi.org/10.1061/NHREFO.NHENG-1771

Lee S, Min K (2001) Statistical analysis of landslide susceptibility at Yongin, Korea. Environ Geol 40:1095–1113

Legros F (2002) The mobility of long-runout landslides. Eng Geol 63(3–4):301–331

Li H, Chen Y, Deng S, Chen M, Fang T, Tan H (2019) Eigenvector spatial filtering-based logistic regression for landslide susceptibility assessment. ISPRS Int J Geo Inf 8(8):332. https://doi.org/10.3390/ijgi8080332

Limak Energy (2022) http://www.limakenerji.com.tr/faaliyet-alanlari/uretim/yenilenebilir-enerji/alkumru-hes. Accessed 15 Mar 2024

Liner CL, McGilvery TA (2019) Historical overview of petroleum and seismology. In: The Art and Science of Seismic Interpretation. Springer Briefs in Earth Sciences. Springer, Cham. https://doi.org/10.1007/978-3-030-03998-1_2.

Lombardo L, Mai M (2018) Presenting logistic regression-based landslide susceptibility results. Eng Geol 244:14–24

Malamud BD, Turcotte DL, Guzzetti F, Reichenbach P (2004) Landslide inventories and their statistical properties. Earth Surf Processes Landforms 29:687–711. https://doi.org/10.1002/esp.1064

Maxon JH (1936) Geology of petroleum possibilities of the Hermis dome. MTA Collection no 255, 25

Mehrotra GS, Sarkar S, Dharmaraju R (1991) Landslide hazard assessment in Rishikesh-Tehri area, Garhwal Himalaya, India. In: Bell DH (ed) Proc. 16th Int. Landslide Conference, Balkema, Rotterdam, pp 1001–1007

Moore ID, Grayson RB, Ladson AR (1991) Digital terrain modeling: a review of hydrological, geomorphological, and biological applications. Hydrol Process 5:3–30

Nagarajan R, Roy A, Kumar RV, Mukherjee A, Khire MV (2000) Landslide hazard susceptibility mapping based on terrain and climatic factors for tropical monsoon regions. Bull Eng Geol Env 58:275–287. https://doi.org/10.1007/s100649900032

Nefeslioglu HA, San BT, Gokceoglu C, Duman TY (2012) An assessment on the use of Terra ASTER L3A data in landslide susceptibility mapping. Int J Appl Earth Obs Geoinf 14(1):40–60. https://doi.org/10.1016/j.jag.2011.08.005

Oriard LL, Emmert MW (1980) Short-delay Blasting at Anaconda's Berkeley Open-pit Mine, AIME Annual Meeting Las Vegas NV 60–80.

Ozer BC, Mutlu B, Nefeslioglu HA, Sezer EA, Rouai M, Dekayir A, Gokceoglu C (2020) On the use of hierarchical fuzzy inference systems (HFIS) in expert-based landslide susceptibility mapping: the central part of the Rif Mountains (Morocco). Bull Eng Geol Environ 79:551–568. https://doi.org/10.1007/s10064-019-01548-5

Özgen N, Karadoğan S (2013) Examining hydro-electric power plants in terms of their spatial effects according to SWOT analysis: sample of Alkumru and Kirazlı Dams (Siirt). J Geogr 26:21–45

Özgen N, Tonbul S, Karadoğan S (2005) Siirt çevresinde kıvrımlı yapı elemanları, jeomorfolojik özellikleri ve gelişimi. https://www.researchgate.net/publication/297716670. Accessed 15 Mar 2024

Pachauri AK, Pant M (1992) Landslide hazard mapping based on geological attributes. Eng Geol 32:81–100

Poudyal CP, Chang C, Oh HJ, Lee S (2010) Landslide susceptibility maps comparing frequency ratio and artificial neural networks: a case study from the Nepal Himalaya. Environ Earth Sci 61:1049–1064. https://doi.org/10.1007/s12665-009-0426-5

Pourghasemi HR, Pradhan B, Gokceoglu C (2012) Application of fuzzy logic and analytical hierarchy process (AHP) to landslide susceptibility mapping at Haraz watershed, Iran. Nat Hazards 63:965–996. https://doi.org/10.1007/s11069-012-0217-2

Pradhan B, Sezer EA, Gokceoglu C, Buchroithner MF (2010) Landslide susceptibility mapping by neuro-fuzzy approach in a landslide-prone area (Cameron Highlands, Malaysia). IEEE Trans Geosci Remote Sens 48(12):4164–4177. https://doi.org/10.1109/TGRS.2010.2050328

Qiu H, Hu S, Yang D, He Y, Pei Y, Kamp U (2021) Comparing landslide size probability distribution at the landscape scale (Loess Plateau and the Qinba Mountains, Central China) using double Pareto and inverse gamma. Bull Eng Geol Environ 80:1035–1046. https://doi.org/10.1007/s10064-020-02037-w

Randomized Search CV (2023) https://scikitlearn.org/stable/modules/generated/sklearn.model_selection.RandomizedSearchCV.html. Accessed 30 Dec 2023

Scikit-learn (2023) Python Library. https://scikitlearn.org/stable/modules/generated/sklearn.ensemble.RandomForestClassifier.html. Accessed 30 Dec 2023

Şenel M (2007) 1:100.000 scale Turkish geological maps, M48 Quadrangle. Publication of General Directorate of the Mineral Research and Exploration, Ankara, Turkey: Department of Geological Research.

Shirvani Z (2020) A holistic analysis for landslide susceptibility mapping applying geographic object-based random forest: A comparison between protected and non-protected forests. Remote Sens 12(3):434. https://doi.org/10.3390/rs12030434

Tanyas H, van Westen CJ, Allstadt KE, Jibson RW (2018) Factors controlling landslide frequency–area distributions. Earth Surf Process Landforms 44:900–917. https://doi.org/10.1002/esp.4543

Tsangaratos P, Benardos A (2014) Estimating landslide susceptibility through an artificial neural network classifier. Nat Hazards 74:1489–1516. https://doi.org/10.1007/s11069-014-1245-x

van Westen C, van Asch T, Soeters R (2005) Landslide hazard and risk zonation—why is it still so difficult? Bull Eng Geol Environ 65:167–184. https://doi.org/10.1007/s10064-005-0023-0

Xing X, Wu C, Li J, Li X, Zhang L, He R (2021) Susceptibility assessment for rainfall-induced landslides using a revised logistic regression method. Nat Hazards 106:97–117. https://doi.org/10.1007/s11069-020-04452-4

Xiong S, Shi W, Wang Y, Zhu C, Yu X (2022) Deformation and failure process of slope caused by underground mining: a case study of Pusa Collapse in Nayong County Guizhou Province, China. Geofluids. https://doi.org/10.1155/2022/1592703

Yılmaz A, Adamia S, Yılmaz H (2014) Comparisons of the suture zones along a geo-traverse from the Scythian Platform to the Arabian Platform. Geosci Front 5:855–875. https://doi.org/10.1016/j.gsf.2013.10.004

Zhao Z, Liu ZY, Xu C (2021) Slope unit-based landslide susceptibility mapping using certainty factor, support vector machine, random forest, CF-SVM and CF-RF models. Front Earth Sci 9:589630. https://doi.org/10.3389/feart.2021.589630